SUPP. TABLE 1 : Clinical information of human subjects. Vitreous was collected either in the right (OD) or left (OS) eye of patients with epiretinal membrane (control) and proliferative diabetic retinopathy (PDR).

Human Vitreous	I.D.	Gender	Age	Eye Collected	Disease Status	Past Medical History	Medication
Epiretinal membrane (ERM)	**14**	F	46	**OS**	Control	-	-
	15	F	84	**OD**	Control	Hypertension, Dyslipidemia	Warfarin, Fluoxetine
	16	M	78	**OS**	Control	Hypertension, Dyslipidemia, Coronary artery disease, Gout, Diabetes Type 2, Atrial fibrillation	Warfarin
	108	M	57	**OS**	Control	Hypertension	-
	***136**	M	68	**OD**	Control	Diabetes Type 1	-
Proliferative diabetic retinopathy (PDR)	**85**	M	74	**OD**	Active with vitreous hemorrhage and tractional retinal detachments	Diabetes Type 2, Dyslipidemia, Hypertension, stroke, Coronary artery disease	Warfarin
	***126**	F	79	**OS**	Active with neovascular glaucoma	Diabetes Type 2, Hemodialysis, Hypertension, Coronary artery disease	-
	124	M	35	**OD**	Active with vitreous hemorrhage and tractional retinal detachments	Diabetes Type 2	-
	86	F	78	**OD**	Active with vitreous hemorrhage	Diabetes Type 2, Dyslipidemia, Hypertension, Renal insufficiency	-
	142	M	36	**OD**	Active with tractional retinal detachments	Diabetes Type 2, Stroke, Renal insufficiency	-
	***153**	M	45	**OD**	Active with macular edema and pre-retinal hemorrhage	Diabetes Type 2, Dyslipidemia, Hypertension	-
	87	F	72	**OS**	Active with vitreous hemorrhage	Diabetes Type 2, Hypertension	Warfarin
	***144**	F	81	**OD**	Active with vitreous hemorrhage and cataract	Diabetes Type 2, Hypertension, Iron-deficiency anaemia, dyslipidemia	Vitamin B12, Acetylsalicylic Acid
	77	M	73	**OS**	Active with vitreous hemorrhage	Diabetes Type 2	-
	76	M	80	**OS**	Active with vitreous hemorrhage	Diabetes Type 2, Hypertension, Coronary artery disease	-

*Patient ID 136, 126, 153 and 144 were detected as outliers by MetaboAnalyst Random Forest analysis and removed from the final analysis

Supplemental Figure 1

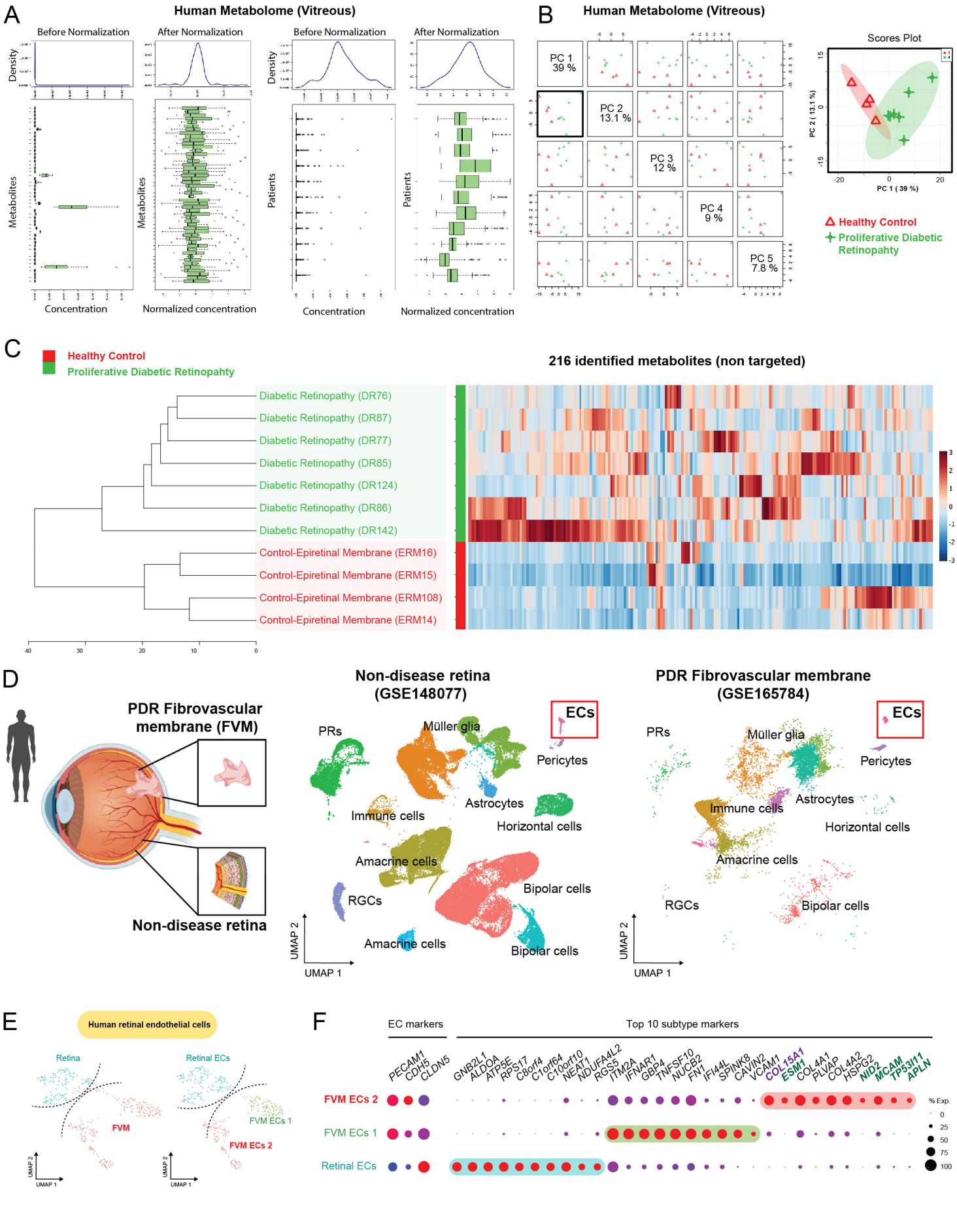

Supplemental Figure 1

A. Normalization of vitreous metabolomics data (see method) showing the distribution of metabolites (left) and patient samples (right).

B. Principal component analysis of vitreous metabolomics data across control (red, n=4) and proliferative diabetic retinopathy (green, n=7) patients.

C. Heatmap clustering of all metabolites across control (red) and proliferative diabetic retinopathy (green) patients.

D. UMAP of publicaly obtained scRNAseq integrated datasets of human post-mortem retina (GSE148007) and fibrovascular membranes (FVM) from human patients with proliferative diabetic retinopathy (GSE165784).

E. UMAP of endothelial subclusters from heatlhy and FVM derived-human retinal sample (EC subset from S1D).

F. Dotplot of top 10 markers for the 3 identified EC subclusters, showing the presence of an FVM endothelial subcluster (FVM ECs 2) expressing gene markers of neovascular ECs (ESM1, TP53I11, APLN, PLVAP).

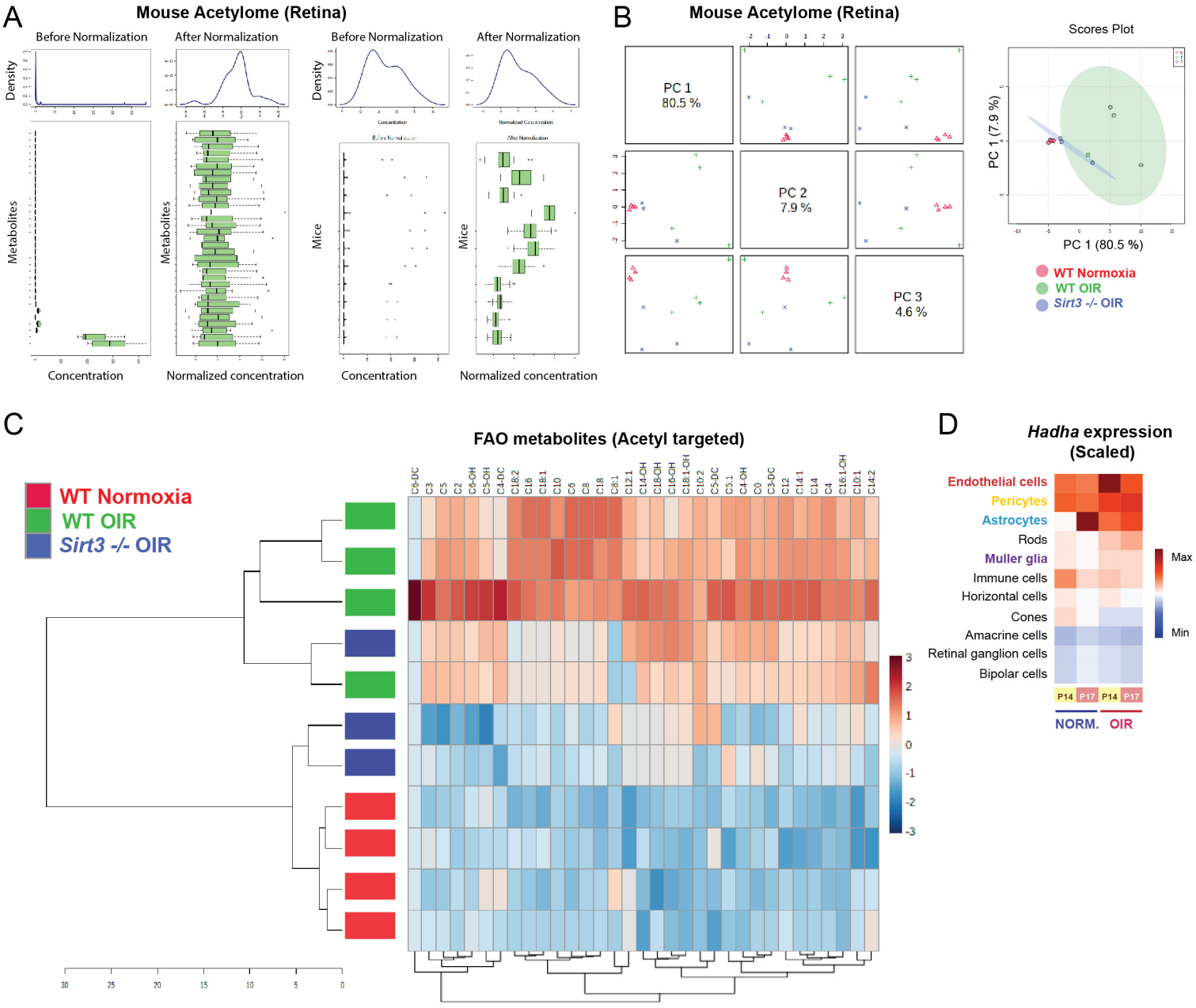

Supplemental Figure 2

A. Normalization of retinal lipidomics data showing the distribution of metabolites (left) and retinal samples (right) from WT normoxia (n=4), WT OIR (n=4) and *Sirt3*$^{-/-}$ OIR (n=3) P14 mice.

B. Principal component analysis of retinal lipidomics data across WT normoxia (red), WT OIR (green) and *Sirt3*$^{-/-}$ OIR (blue) P14 mice.

C. Heatmap clustering of retinal samples based on all lipidomics metabolites for WT normoxia (red), WT OIR (green) and *Sirt3*$^{-/-}$ OIR (blue) P14 mice.

D. Expression levels of *Hadha* (Hydroxyacyl-CoA Dehydrogenase Trifunctional Multienzyme Complex Subunit Alpha), which encodes a subunit of the mitochondrial trifunctional protein essential for acyl-carnitine b-oxidation, from single-cell RNAseq analysis of normoxic and OIR mouse retina at P14 and P17 (GEO accession number GSE150703).

Supplemental Figure 3

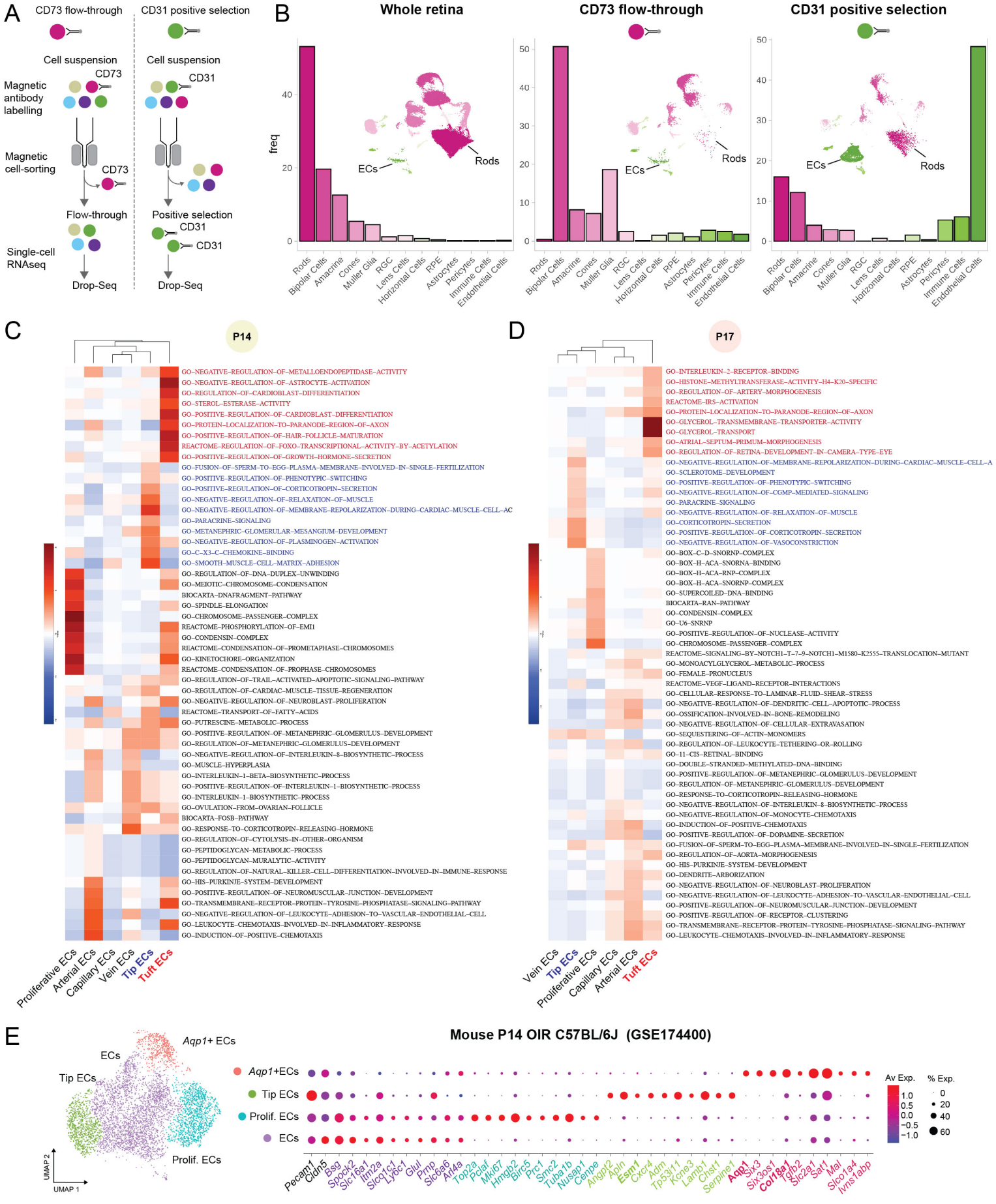

Supplemental Figure 3
A. Two different approaches to enrich cell types of interest for single-cell RNAseq analysis, using magnetic cell isolation technology (MACS, Miltenyi Biotec). Retinal cell suspension can either be depleted of rods (CD73 antibody) or enriched for endothelial cells (CD31 antibody)
B. Single-cell RNAseq illustrating the cell type distribution using whole retina compared to CD73 depleted or CD31 enriched cell suspensions.
C and D. Heatmap of pathway enrichment based on GSVA analysis of scRNAseq data showing the normalized GSVA score for the most enriched pathways in each endothelial subtype of OIR retina at P14 and P17.
E. UMAP of publicly obtained scRNAseq of P14 retina from C57B6/6J mice exposed to OIR (GSE174400) showing the presence of *Aqp1*+ EC subcluster (*Aqp1, Col18a1*).

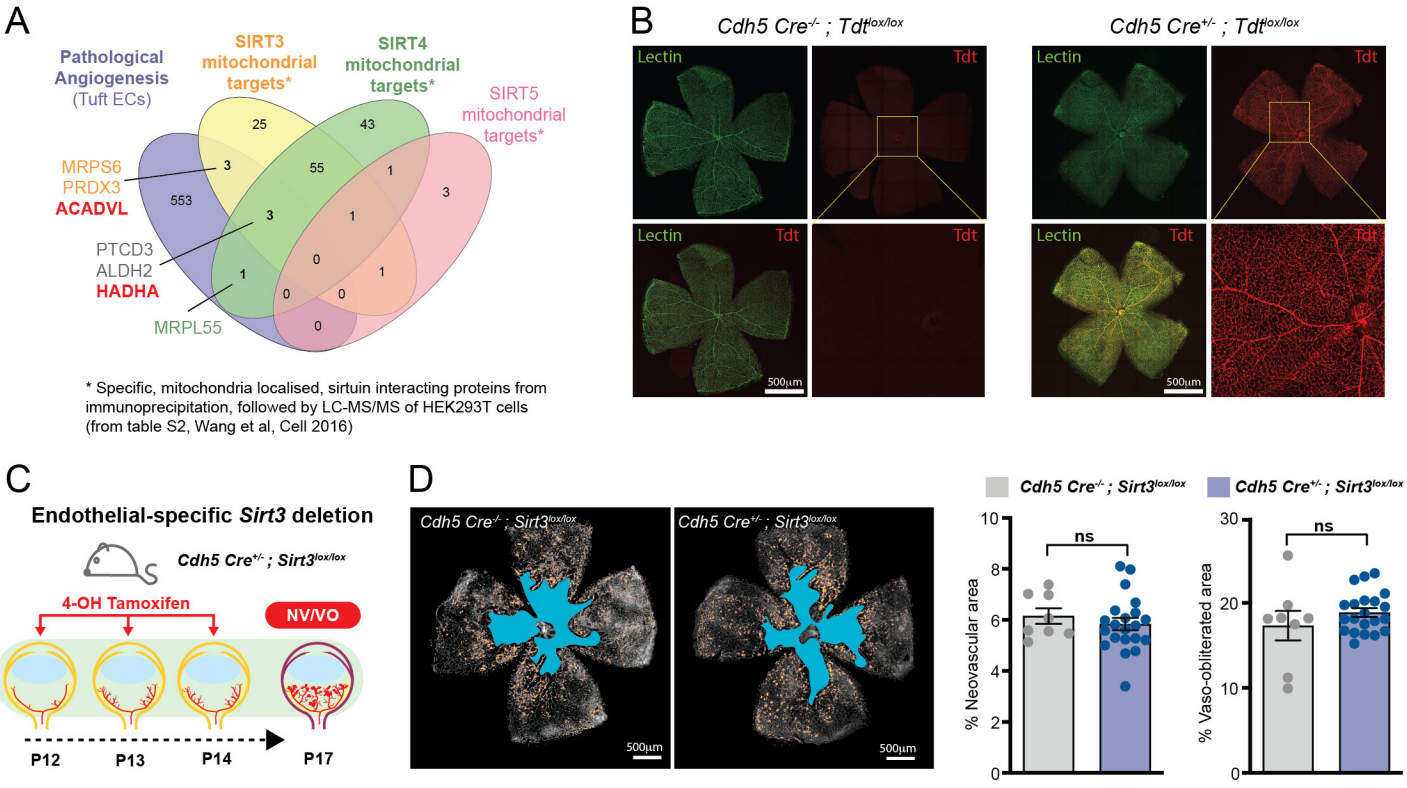

Supplemental Figure 4

A. Overlap between mitochondrial sirtuins (SIRT 3,4,5) interacting proteins (from HEK293T cells) and differentially expressed genes (DEG) in tuft and tip EC from OIR retinas (P17); 6 DEG in tuft EC, including ACADVL and HADHA, were proteins known to directly interact with SIRT3.

B. Retinal flatmounts of tamoxifen-injected Cdh5-CreERT2 expressing mice, or not, and bred with tdTomato$^{lox/lox}$ (Tdt) reporter mice. Endothelial expression of Cdh5-CreERT2 by 4-OH tamoxifen (red) localized to retinal vessels (lectin, green).

C. Graphical representation of the experimental strategy to induce EC-specific deletion of Sirt3 during the neovascularization period of OIR. *Cdh5-CreERT2$^{-/-}$; Sirt3$^{lox/lox}$* and *Cdh5-CreERT2$^{+/-}$; Sirt3$^{lox/lox}$* mice were treated from P12 to P14 with daily injections of 4-OH Tamoxifen (5 µg).

D. Lectin-stained retinal flat-mount of P17 *Cdh5-CreERT2$^{-/-}$; Sirt3$^{lox/lox}$* (n=8 retinas) and *Cdh5-CreERT2$^{+/-}$; Sirt3$^{lox/lox}$* mice (n=21 retinas) exposed to the OIR model; vaso-obliterated (VO, blue) and neovascular (NV, yellow) areas are highlighted. Bar graph represents VO and NV areas relative to total retinal areas (unpaired Student t-test, ns: P-value > 0.05).

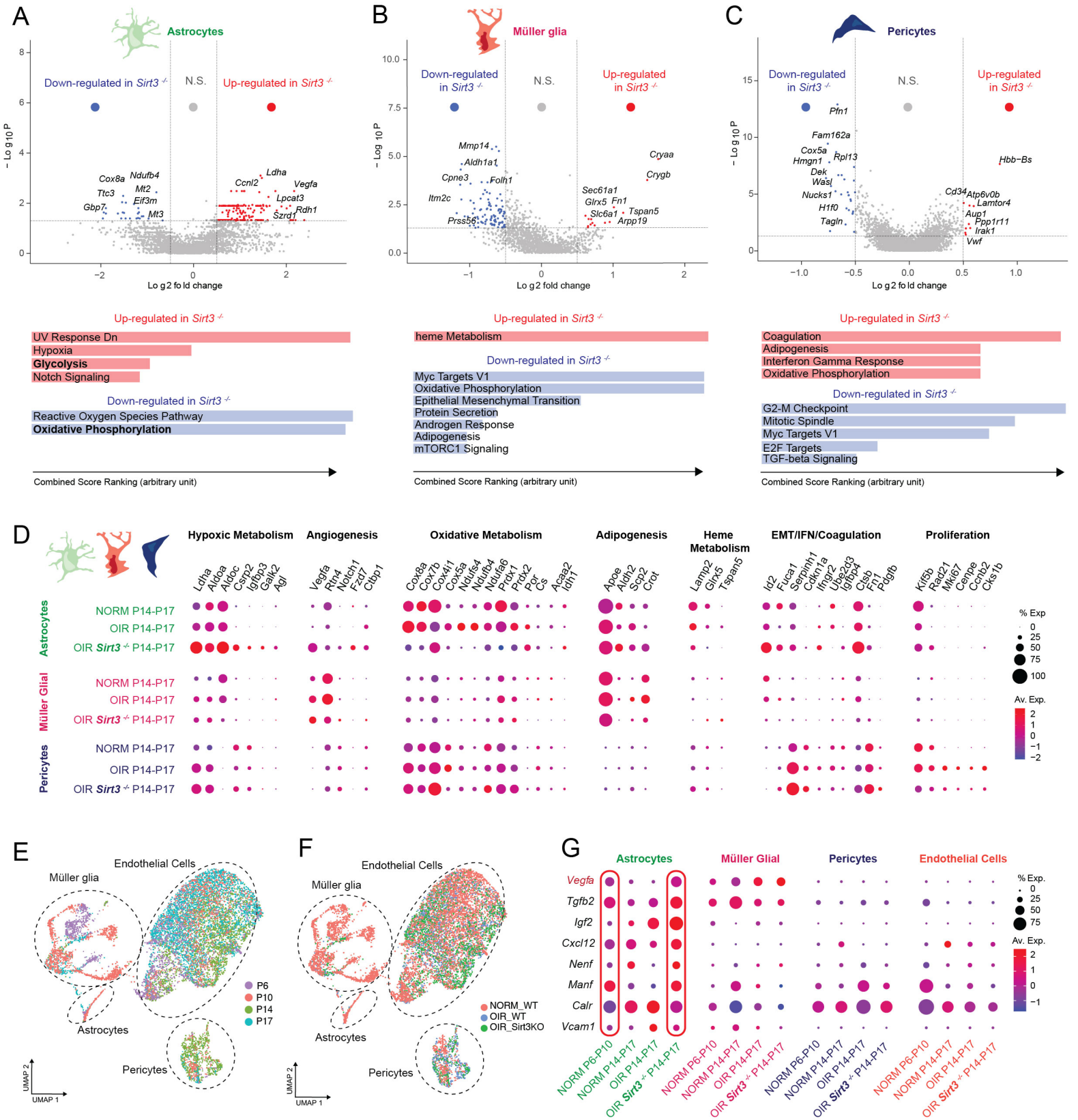

Supplemental Figure 5

A-C. Volcano plot of differentially expressed genes between OIR WT and *Sirt3*$^{-/-}$ astrocytes, muller glia and pericytes (P value <0.05, absolute log2FC > 0.25, non-parametric Wilcoxon rank sum test, excluding genes expressed in less than 10% of cells in the given cell type), and their asscoaited pathways from EnrichR.

D. Dotplot of differentially expressed genes between OIR WT and *Sirt3*$^{-/-}$ in cells of the vascular unit in OIR compared to normoxia.

E.F. UMAP of integrated single-cell RNAseq from publically available mouse retinal P6-10 dataset (10X, GSE175895) with the current P14-17 dataset.

G. Dot plot representing the expression of selected ligands found differentially expressed between cells of the vascular unit in WT and *Sirt3*$^{-/-}$ retinas using NicheNet analysis, during development (P6-10) and compared to OIR (P14-17).

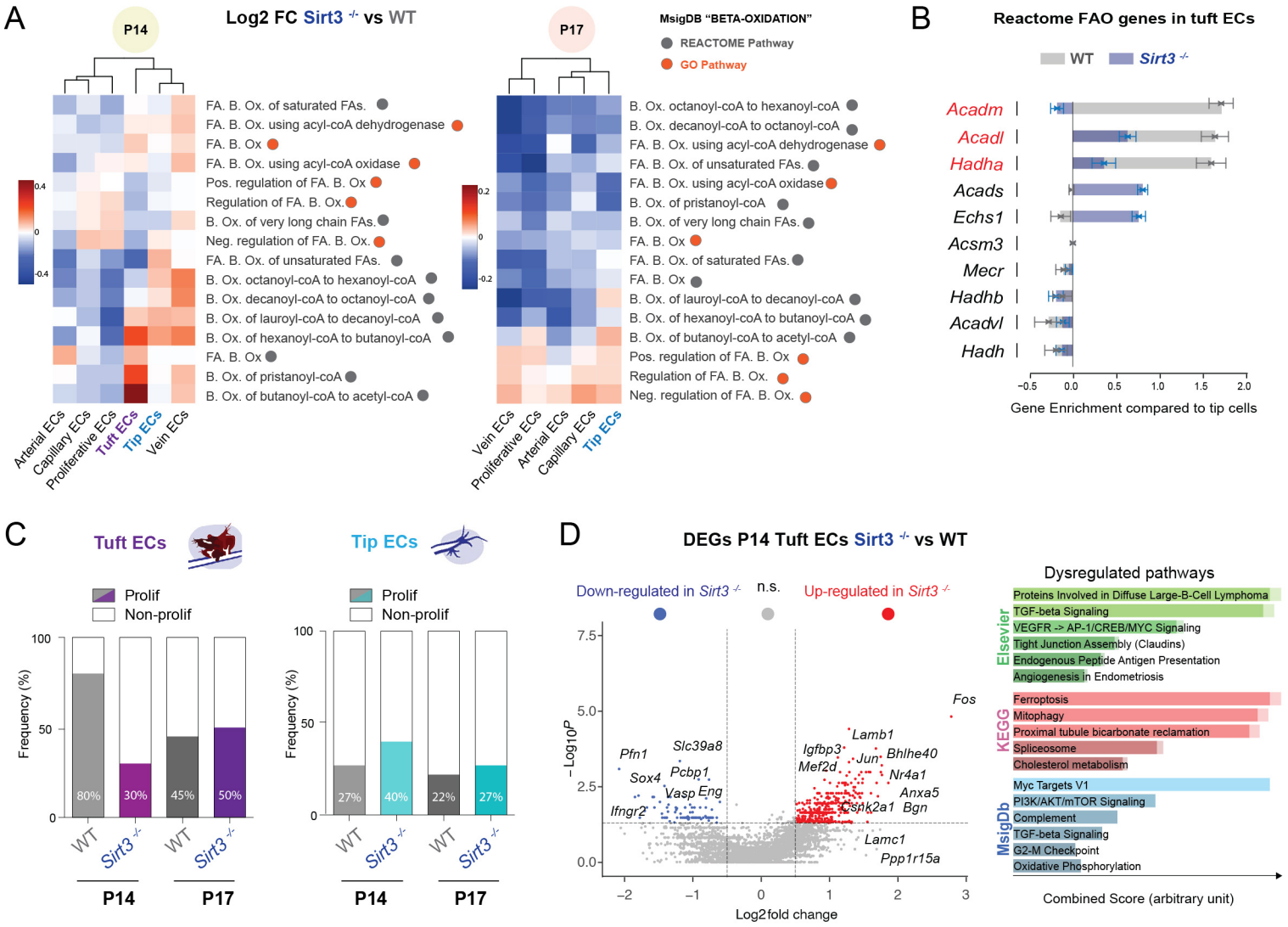

Supplemental Figure 6

A. Heatmap of normalized GSVA score log2 fold-change between OIR WT and *Sirt3*$^{-/-}$ ECS subtypes for several FAO pathways from the GO and REACTOME Molecular Signature database at P14 and P17.

B. Comparison by Qusage of pathway enrichment in tuft ECs relative to tip cells for the REACTOME Fatty-acid oxidation pathways in P14 OIR WT and *Sirt3*$^{-/-}$ retina. Qusage Gene Set Enrichment-type test uses the Variance Inflation Factor technique and quantification of gene set activity with a complete probability density function.

C. Percent of non-proliferative (G1) and proliferative cells (S, G2/M) amongst tip and tuft ECs per genotype and time point.

D. Volcano plot of differentially expressed genes between P14 OIR WT and *Sirt3*$^{-/-}$ tuft ECs (P value <0.05, absolute log2FC > 0.5, non-parametric Wilcoxon rank sum test, excluding genes expressed in less than 10% of cells in the given cell type), with the corresponding enriched pathways from EnrichR.